Solid-state NMR study of structural heterogeneity of the apo WT mouse TSPO reconstituted in liposomes

Luminita Duma, Lucile Senicourt, Baptiste Rigaud, Vassilios Papadopoulos, Jean-Jacques Lacapère

Solid-state NMR study of structural heterogeneity of the apo WT mouse TSPO reconstituted in liposomes

Luminita Duma[a], Lucile Senicourt[b], Baptiste Rigaud[c], Vassilios Papadopoulos[d], Jean-Jacques Lacapère[b]

[a] Champagne-Ardenne University, CNRS, ICMR UMR 7312, Reims, France;
[b] Sorbonne Université, Ecole Normale Supérieure, PSL University, CNRS, Laboratoire des Biomolécules (LBM), 4 Place Jussieu, F-75005 Paris, France;
[c] CNRS Institut des Matériaux de Paris Centre (FR2482), 4 Place Jussieu, 75005 Paris, France;
[d] Department of Pharmacology and Pharmaceutical Sciences, School of Pharmacy, University of Southern California, Los Angeles, CA 90089, USA

Corresponding author: luminita.duma@univ-reims.fr

Highlights

- In lipids, mTSPO has several coexisting conformations in the absence of the ligand
- Lipids and mTSPO spectra reveal flexible fragments even at low temperature
- Partial assignment of residue types of apo mTSPO was obtained in lipids
- Apo mTSPO shows partial structural identities with atomic solution NMR structure

Graphical abstract

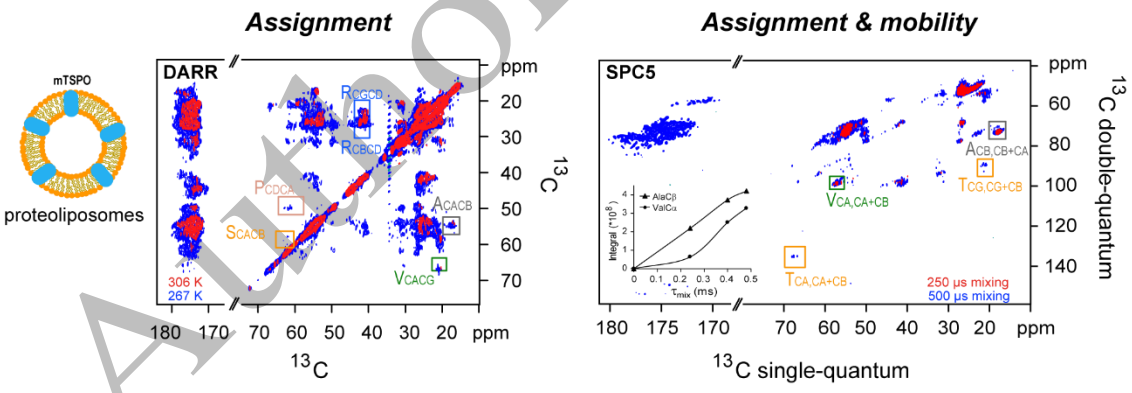

Keywords: solid-state NMR, membrane protein, TSPO, proteoliposomes, conformational mobility

Abbreviations:
1D one-dimension;
2D two-dimension;
3D three-dimension;
CC carbon-carbon;
NC nitrogen-carbon;
NMR Nuclear Magnetic Resonance;
ssNMR solid-state NMR;
MAS Magic-Angle Spinning;
DARR Dipolar-Assisted Rotational Resonance;
PDSD Proton-Driven Spin Diffusion;
INEPT Insensitive Nuclei Enhancement by Polarization Transfer;
INADEQUATE Incredible Natural Abundance DoublE QUAntum Transfer Experiment;
CP Cross Polarisation;
DQ - SQ Double Quantum Single Quantum;
SPC5 Supercycled Permutationally offset-Compensated C5;
HSQC Heteronuclear Single Quantum Coherence;
TSPO TranSlocator PrOtein;
mTSPO mouse TSPO;
*Bc*TSPO *Bacillus cereus* TSPO;
*Rs*TSPO *Rhodobacter sphaeroides* TSPO;
PK 11195 N-butan-2-yl-1-(2-chlorophenyl)-N-methylisoquinoline-3-carboxamide;
DMPC Dimyristoil phosphatidyl choline;
DMPE Dimyristoyl phosphoethanolamine;
TM Transmembrane;
WT Wild Type;

Abstract
In the last decades, ligand binding to human TSPO has been largely used in clinical neuroimaging, but little is known about the interaction mechanism. Protein conformational mobility plays a key role in the ligand recognition and both, ligand-free and ligand-bound structures, are mandatory for characterizing the molecular binding mechanism. In the absence of crystals for mammalian TSPO, we have exploited solid-state nuclear magnetic resonance (ssNMR) spectroscopy under magic-angle spinning (MAS) to study the apo form of recombinant mouse TSPO (mTSPO) reconstituted in lipids. This environment has been previously described to permit binding of its high-affinity drug ligand PK11195 and appears therefore favourable for the study of molecular dynamics. We have optimized the physical conditions to get the best resolution for MAS ssNMR spectra of the ligand-free mTSPO. We have compared and combined various ssNMR spectra to get dynamical information either for the lipids or for the mTSPO. Partial assignment of residue types suggests few agreements with the published solution NMR assignment of the PK11195-bound mTSPO in DPC detergent. Moreover, we were able to observe some lateral chains of aromatic residues that were not assigned in solution. ^{13}C double-quantum NMR spectroscopy shows remarkable dynamics for ligand-free mTSPO in lipids which may have significant implications on the recognition of the ligand and/or other protein partners.

1. Introduction

Membrane proteins are medically relevant entities and their structure determination is therefore essential for the understanding of the mechanisms of action and the design of inhibitors or biomarkers. Significant technological and sample preparation advances have been made over the years but their structure determination within their native or semi-native environment [1] remains challenging by X-ray crystallography [2], cryo-electron microscopy [3] and solution NMR [4]. The field of membrane proteins within lipid bilayers by solid-state nuclear magnetic resonance (ssNMR) has also seen a continuous and important progress during the last decades with various biologically and medically relevant systems investigated: ABC transporter BmrA [5,6], β-barrel AlkL [7], BamC lipoprotein [8], envelope protein E of the SARS-CoC-2 [9], human VDAC [10] to give just few examples. The access to magnetic fields as high as 1.2 GHz and ultra-fast (above 100 kHz) spinning CPMAS probes fostered even more the investigation of such challenging biological systems [11,12]. Most of membrane protein structures determined by NMR were for systems in detergent and only few in membrane lipids [13–16]. The structures of more than 1400 membrane proteins have been registered to date [17] and it is expected that the combined use of the techniques mentioned previously together with mass spectrometry, small-angle neutron diffraction, molecular dynamics simulations [18] would contribute to a better understanding of their function and mechanisms of such challenging biological molecules which are the membrane proteins.

TSPO is an 18 kDa membrane protein highly conserved from bacteria to mammals [19]. Atomic structures of mouse TSPO (mTSPO) has been obtained by solution NMR in detergent after stabilization by the presence of a high affinity drug ligand, the PK11195 [20]. In the absence of the ligand, the protein is highly flexible and presents several coexisting conformations [21] that prevent structure determination. When reincorporated in liposomes, the mTSPO exhibits high affinities for its ligands like PK11195 and cholesterol [22], and ssNMR studies have shown that cholesterol mediates allosteric regulations of the ligand bound protein [23]. In 2021, Rivière et al. explored by ssNMR the impact of three different lipid composition on the structure of mTSPO embedded into lipid bilayers in the presence and in the absence of the ligand and further confirmed how cholesterol can affect the tertiary and quaternary mTSPO structure [24]. Despite these efforts, detailed high-resolution atomic data of mTSPO in its native-lipid environment without ligand, that would permit to directly characterize the structural changes mediated by ligand binding that are linked to TSPO functional properties, are still missing. It has to be mentioned that bacterial TSPO structures obtained by X-ray crystallography both in the absence (apo form) and in the presence (holo form) of ligands do not provide any information on the functional properties of the TSPO protein since the atomic structures do not reveal great changes between the ligand-free and ligand-bound structures [25,26]. As previously discussed, given the lack of changes between the X-ray structures of the apo and holo forms of TSPO, only dynamics aspects could explain how the ligand enters the binding cavity [27]. Indeed, this might be due to the fact that crystals formation captures only a specific conformation, such as that observed in the crystal packing of the Ca ATPase [28].

Here, we attempt to study the mTSPO in a lipid environment in the absence of the ligand by ssNMR using proteoliposomes [22,29–32] by providing complementary

information to the work by Rivière et al. [24]. The tertiary structure determination by ssNMR of membrane proteins reconstituted in proteoliposomes first requires the acquisition of several types of two-dimension (2D) and three-dimension (3D) spectra (2D CC, NCO, NCA, CHHC, NHHC, 3D NCACX, NCOCX, CONCA) to identify spin systems and sequential assignments. The 3D heteronuclear experiments are essential as they remove correlation degeneracies and give *intra*- (NCACX) and *inter*-residue (NCOCX, CONCA) correlations required for the identification of backbone and sidechain connectivities. Generally, CC transfers rely on proton-driven spin diffusion (PDSD) or dipolar-assisted rotational recoupling (DARR) methods [33], depending on the spinning frequency and the magnetic field. Instead, one-bond NC transfers are often performed with SPECIFIC-cross-polarisation (CP) recoupling techniques [34]. Spinning frequencies as fast as 100 kHz combined with ^{1}H-direct detection methods lead to increased sensitivity and ^{1}H linewidths which rendered these protocols applicable to some of these challenging membrane proteins [35].

Improved sensitivity and spectral resolution can be achieved for membrane proteins if several experimental conditions are optimized. For example, the choice of lipid-to-protein ratio (LPR) depends on protein characteristics and can have critical consequences on the quality of NMR spectra. An isotopically labelled membrane protein co-purified with lipids (also labelled) brings strong lipid signals in the NMR spectra. Instead, a labelled membrane protein reconstituted in natural lipids (proteoliposomes) will give smaller lipid signals but remains nevertheless governed by the LPR used [32,36]. Once the NMR rotor filled with proteoliposomes [30], the best physical parameters (such as temperature) and the optimal pulse sequences for spectra recording need to be chosen in order to reach good sensitivity and spectral resolution. Previous data on GB1 and Vpu recorded at different temperatures have shown their importance for the optimization of NMR sensitivity [37,38]. Most of the ssNMR data acquired on membrane proteins in lipids are based on CP rather than the INEPT element [39–41] since dipolar coupling transfer (*through space*) is expected to be more efficient than scalar (*through bond*) one. Scalar-based methods such as INEPT and notably INADEQUATE have been shown to work well for microcrystalline super-oxide dismutase under ultrafast magic-angle spinning [42]. The efficiency of dipolar-based transfers, such as SPECIFIC-CP, may be affected by molecular motions on intermediate timescale [43] and therefore lead to reduced sensitivity of ssNMR spectra when applied to non-crystalline samples, such as some membrane proteins and amyloid fibrils. Among the various experiments that can probe molecular dynamics by ssNMR, ^{13}C – ^{13}C double-quantum spectroscopy [44] appears particularly useful for ^{13}C-labelled biomolecules since it benefits of the high dispersion of the ^{13}C chemical shifts but also the increased resolution of the double-quantum (DQ) dimension. Combined with ^{1}H detection under ultrafast MAS, the DQ ^{13}C spectroscopy was notably successful for the sequential assignment of HET-s(218–289) amyloid fibrils [45].

We showed previously the successful reconstitution of apo mTSPO protein into DMPC/DMPE 9/1 liposomes with the first preliminary ^{13}C – ^{13}C DARR and NCO, NCA spectra [30,32]. We present herein magic-angle spinning ssNMR studies which explore the different transfer elements described previously on the mTSPO protein reconstituted in liposomes. We will also overview the protocol which lead to a stable and relatively homogenous mTSPO sample and the corresponding spectra. Chemical shift correlation spectra at 11.7 T (500 MHz ^{1}H Larmor frequency) and 10 kHz spinning frequency have

been employed to perform a partial assignment of the different residue type regions. The effect of temperature on ^{13}C or ^{15}N CPMAS, ^{13}C – ^{13}C DARR or ^{15}N – ^{13}C correlation spectra is illustrated. Moreover, ^{13}C – ^{13}C DQ – SQ spectra have been recorded to probe molecular motion of different regions of the protein. The obtained results could provide possible answers to questions raised in previous works about flexible fragments of the monomeric mTSPO and of the binding pocket [46] but also in the case of the dimer mTSPO in the presence of cholesterol [23].

2. Material and methods

Mouse TSPO expression, purification and reconstitution in liposomes*:* The protocols were described in detail elsewhere [30]. In summary, the recombinant mTSPO protein was expressed in *Escherichia coli* BL21 (DE3) bacteria in lysogeny browth (LB) medium (1% w/v tryptone, 0.5% yeast extract, and 0.5% NaCl) and purified by His-binding Ni-NTA chelation resin in the presence of 1% SDS. Expression protein level was estimated based on the absorbance measured at 280 nm wavelength (extinction coefficient 3.88 $(mg/ml)^{-1}cm^{-1}$ calculated from the mTSPO amino acid sequence including the polyhistidine tag) whereas the protein purity was verified by SDS-PAGE (12% acrylamide). The reconstitution of the mTSPO in a lipid environment is performed in three steps: i) solubilisation of the protein in the SDS detergent; ii) addition of lipids (DMPC/DMPE 9/1 w/w) to form a ternary protein-lipid-detergent complex; iii) SDS detergent removal in a controlled way using bio-beads [22]. Proteoliposomes were thus formed in few hours. Different reconstitutions have been performed with apo WT mTSPO at lipid-to-protein ratios were between 1 and 3 (w/w) (i.e., ~30 to 90 molar ratio). Since at high LPR ratio a strong ^{13}C lipid signal is present in the carbon spectra thus preventing a good protein signal detection, a LPR ratio of 1.5 w/w was used for the recording of all ssNMR spectra presented herein. Various methods have been used to validate the correct reconstitution of mTSPO into lipid bilayers: absorbance, intrinsic fluorescence, dynamic light scattering, cryo-electron microscopy and ssNMR) [22,29,30,32,47]. Cryo-electron microscopy images at different steps of the reconstitution protocol have demonstrated the formation of proteoliposomes without aggregates [30]. The correct reconstitution of mTSPO into DMPC/DMPE lipid bilayers has been previously assessed by recording the ^{13}C – ^{13}C correlation spectra in the presence and in the absence of the high-affinity PK11195 ligand [32]. The addition of the PK11195 ligand has a dramatic effect on the ^{13}C – ^{13}C correlation spectrum by improved chemical shift dispersion and increased number of observed correlations which confirms the ligand induced structure stabilisation.

NMR spectroscopy: All NMR data were recorded on a Bruker spectrometer (500 MHz ^{1}H Larmor frequency) equipped with a 4 mm triple resonance probe head. A 10 kHz MAS rate was used for all experiments. The sample temperature was regulated with a BCU-Xtreme cooling unit using either 270 l/h (above 295 K) and 935 l/h (below 295 K). For CPMAS experiments, a 2.58 μs ^{1}H 90° pulse was followed by 800 μs (^{13}C CPMAS) or 1 ms (^{15}N CPMAS) contact time with ramped shape pulse (ramp70100.100) on ^{1}H [48]. The recycle delay was set to 2 s. The ^{1}H CP field strength was set to ω_1 = 55 kHz (^{13}C CPMAS) or 35 kHz (^{15}N CPMAS) and matched to the +1 Hartman-Hahn sideband condition. Heteronuclear decoupling based on the SPINAL64 scheme [49] was active on the proton

channel during acquisition at 97 kHz field strength. ^{13}C – ^{13}C spin diffusion assisted by proton irradiation or 2D DARR spectra were recorded at different mixing times (10, 20, 50, 100 ms). The SPECIFIC-CP transfer between ^{15}N and ^{13}CO was performed with 30 kHz a 20% tangent ramp (^{15}N) and 20 kHz (^{13}C). 2D ^{13}C – ^{13}C DQ – SQ SPC5 [50] experiments at different mixing times were recorded at a ^{13}C radio frequency (rf) filed strength of 54 kHz. Data were processed with NMRPipe [51] and visualized with the NMRFAM-Sparky distribution [52]. FANDAS 2.0 software [53] served to create a peak list file readable by Sparky from the published solution NMR mTSPO BMRB (ID 19608) chemical shift assignment in DPC detergent. Assignment of the different amino acid types was performed based on the solution published assignment and estimations made with the PLUQ software [54] on the NMRBOX server [55]. One-dimension (1D) and two-dimension (2D) NMR data were acquired at 261, 267, 272, 278, 283, 289, 295, 300 and 306 K. The sample temperatures were calibrated with lead nitrate, $Pb(NO_3)_2$ [56]. ^{13}C and ^{15}N chemical shifts were externally referenced using adamantane ($\delta(^{13}C)$ = 38.5 ppm for methylene at 295 K) and glycine ($\delta(^{15}N)$ = 32 ppm at 295 K).

3. Results

3.1 Temperature effect upon 1D and 2D MAS NMR spectra

Any NMR study of biomolecules involves suitable [^{13}C, ^{15}N]-labelled material for the protein of interest to resolve the various cross-peaks from the backbone and side-chain nuclei of the protein in the 2D and 3D correlation spectra. One-dimension (1D) ^{13}C CPMAS and INEPT spectra were recorded over a wide range of temperatures (from 261 to 305 K, see Fig S1) for DMPC lipid vesicles and liposomes containing uniformly [^{13}C, ^{15}N]-labelled mTSPO. Since ^{13}C CPMAS exploits the dipolar polarization transfer, these spectra largely report on the rigid domains of the protein or lipids whereas through bond ^{13}C INEPT experiments probe segments in fast motion. For lipid vesicles, we identified all ^{13}C resonances [57] in both INEPT and CPMAS spectra above 15 °C (Fig S1). ^{13}C INEPT spectra show the disappearance of the signals in agreement with lipids immobilization at low temperature (Fig 1a) except for γ-CH_3 of choline (Fig 1e for DMPC chemical structure with nomenclature) whose intensity only decreases with temperature. For the ^{13}C CPMAS spectra, different behaviours are visible depending on the type of carbons (Fig 1b). The intensities of glycerol (G1, G2, G3) and choline α-CH_2 carbons decrease with temperature whereas CH_3 of aliphatic chains increases due to lipid immobilization which leads to more efficient dipolar transfer. Instead, the spectra of proteoliposomes containing mTSPO show lipid resonances with an intensity which is, as expected, attenuated by the protein presence. The INEPT spectra display extra patterns coming from the protein in the region from 40 to 60 ppm (Fig 1c) whereas the profile of ^{13}C resonances in the 20 to 30 ppm region, corresponding to the overlay of lipid and protein resonances, changes from sharp peaks (lipids) to a massive (protein). This suggests that lipids surrounding the protein are less mobile in the presence of the protein compared to the lipids alone. Indeed, most of the narrow carbon resonances disappear except for γ-CH_3 choline and CH_3 of aliphatic chain whose intensity only decreases. As expected, we observe an improved sensitivity of the ^{13}C CPMAS spectra at low temperature (see CO region Fig 1d left) at the expense of the resolution (see aliphatic region Fig 1d right). The change in the chemical shift of 4-11 peak

as a function of temperature is consistent with the previously described gel to liquid phase transition of the DMPC lipids [58]. Therefore, the liposomes preserve the role of lipid phases. Moreover, the reduction of the of mTSPO and lipids intensity in ^{13}C CPMAS as a function of increasing temperature is associated to an increased overall mobility. Indeed, above the lipid-phase transition temperature membrane proteins reconstituted in proteoliposomes undergo rapid lateral and rotational diffusion about the bilayer normal [59,60].

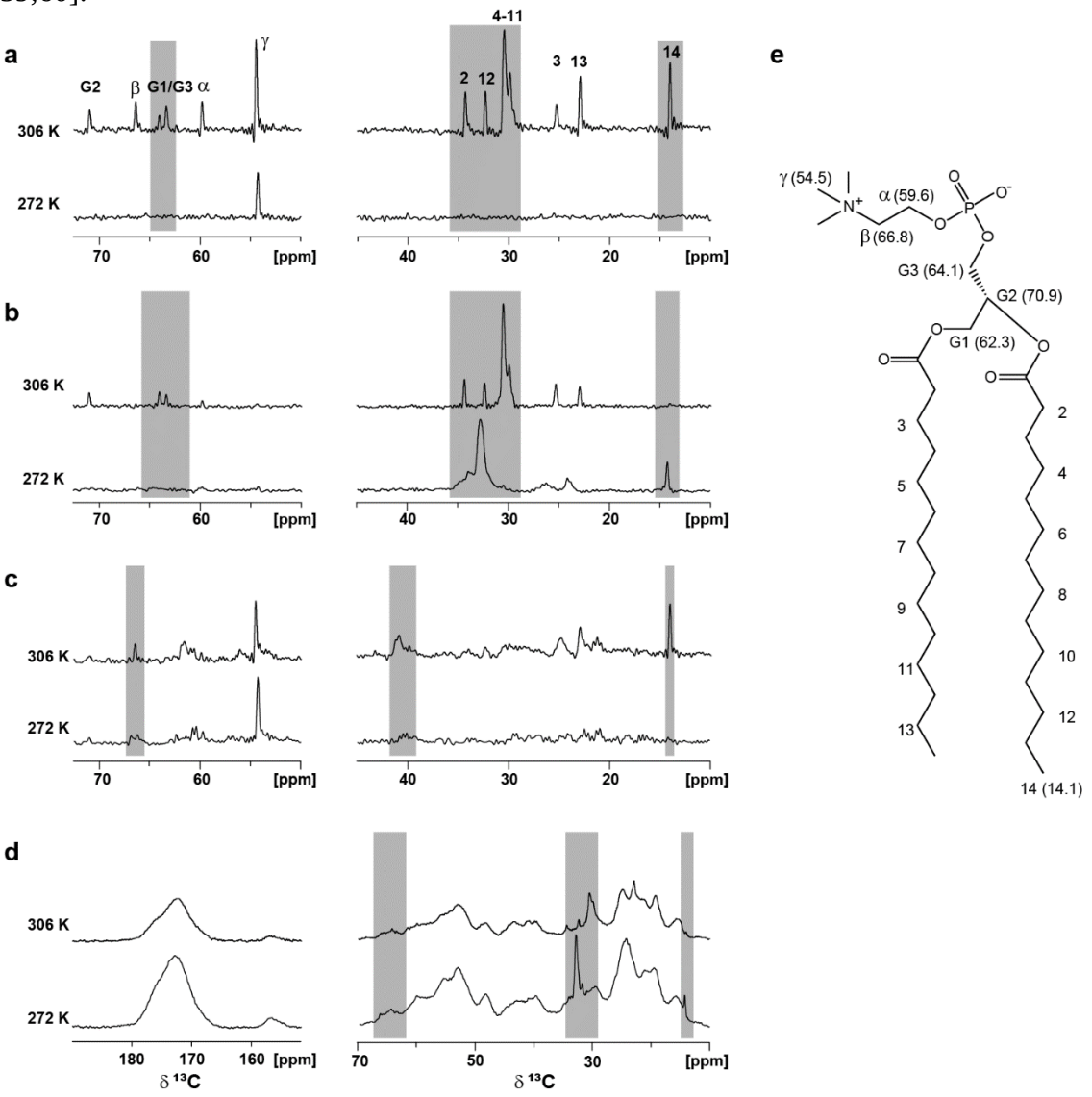

Figure 1: 1D ^{13}C INEPT (a, c) and CPMAS (b, d) spectra of lipid vesicles (a, b) and mTSPO1 in proteoliposomes (c, d) at two temperatures (272 and 306 K). (e) Chemical structure of DMPC with nomenclature and ^{13}C chemical shifts at 306 K for some carbon resonances highlighted on the spectra.

^{15}N CPMAS spectra (Fig 2) of the mTSPO protein were also recorded at 267 and 306 K sample temperature [39,61]. Cooling the sample temperature below the lipids gel to liquid-crystal phase transition leads to an increased sensitivity of the ^{15}N CPMAS spectrum due to an improved ^{1}H - ^{15}N dipolar cross-polarization transfer. However, owing to the low

sensitivity of the ^{15}N CPMAS spectra, the characteristic Lys and Arg side chain nitrogens, as well as the Pro nitrogen [61] are not clearly visible within the temperature range explored.

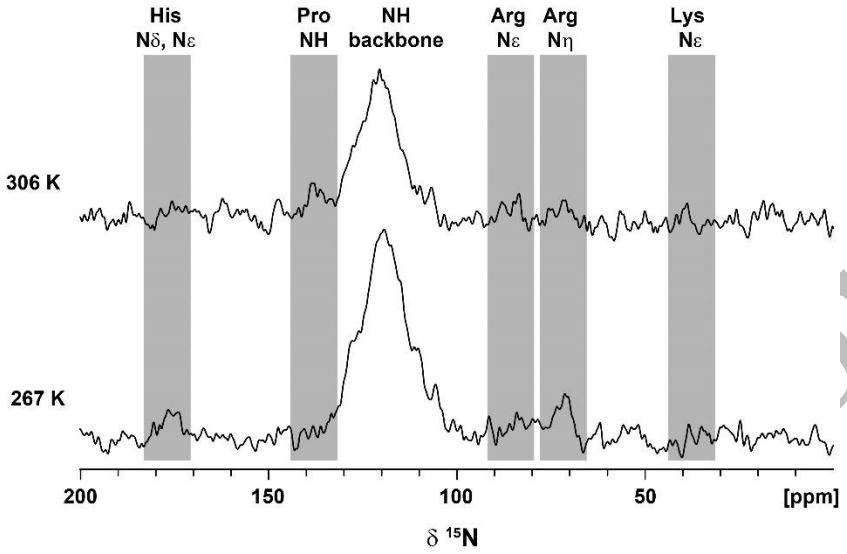

Figure 2: 1D ^{15}N CPMAS spectra of mTSPO at 267 and 306 K sample temperature. The expected regions (based on BMRB data) of NH Pro, Nε and Nη Arg, Nε Lys are highlighted in grey.

In complement to 1D spectra, tow-dimension (2D) ^{13}C - ^{13}C DARR and ^{15}N - ^{13}C NCO spectra were recorded at 267 and 306 K (Fig 3). We choose DARR because it performs better polarization transfer than PDSD notably at high spinning frequency and magnetic fields [62]. DARR scheme relies on the ^{1}H low power rf irradiation fulfilling a rotary-resonance recoupling condition (here the ^{1}H rf power equals the spinning frequency) and has originally been developed for effective band-selective recoupling between carbonyl/aromatic carbons and aliphatic carbons [33]. Fig 3 shows that the polarization transfer is, as expected, more efficient at low temperature, and allows the observation of more cross-peaks for various individual atom pairs. In particular, we clearly detect new cross-peaks correlations in the aromatic and serine regions (Fig 3a, boxed highlighted in blue and green, respectively). 1D traces extracted from the aromatic (Fig 3c) and the ensemble of Cα serine (Fig 3d) regions illustrate this transfer improvement. Fig 3e and 3f displays the effect of the temperature on NCO spectra. Lowering the temperature increases the transfer between N and C since more peaks are observed. However, the crowded spectrum and the poor resolution avoid an easy assignment. The limited resolution arises from the loss of signal in the indirect dimension, due to a fast nitrogen signal decay, which reduces the transfer from nitrogens to carbons. Some ^{15}N – ^{13}C cross-peaks observed at 306 K are not present at 267 K. The temperature variation induces changes in the local atomic environment owing to the protein alone or its interaction with lipids but, since the ^{13}C and ^{15}N nuclei are less sensitive to temperature variations than the ^{1}H, the disappearance of the peaks should have a different origin. Bauer et al. [63] have shown by analysing the ^{13}C – ^{13}C DREAM spectra of the amyloid form of HET-s(218-289) that the solvent-exposed residues suffer most from the temperature-dependent broadening and can disappear completely from the spectrum.

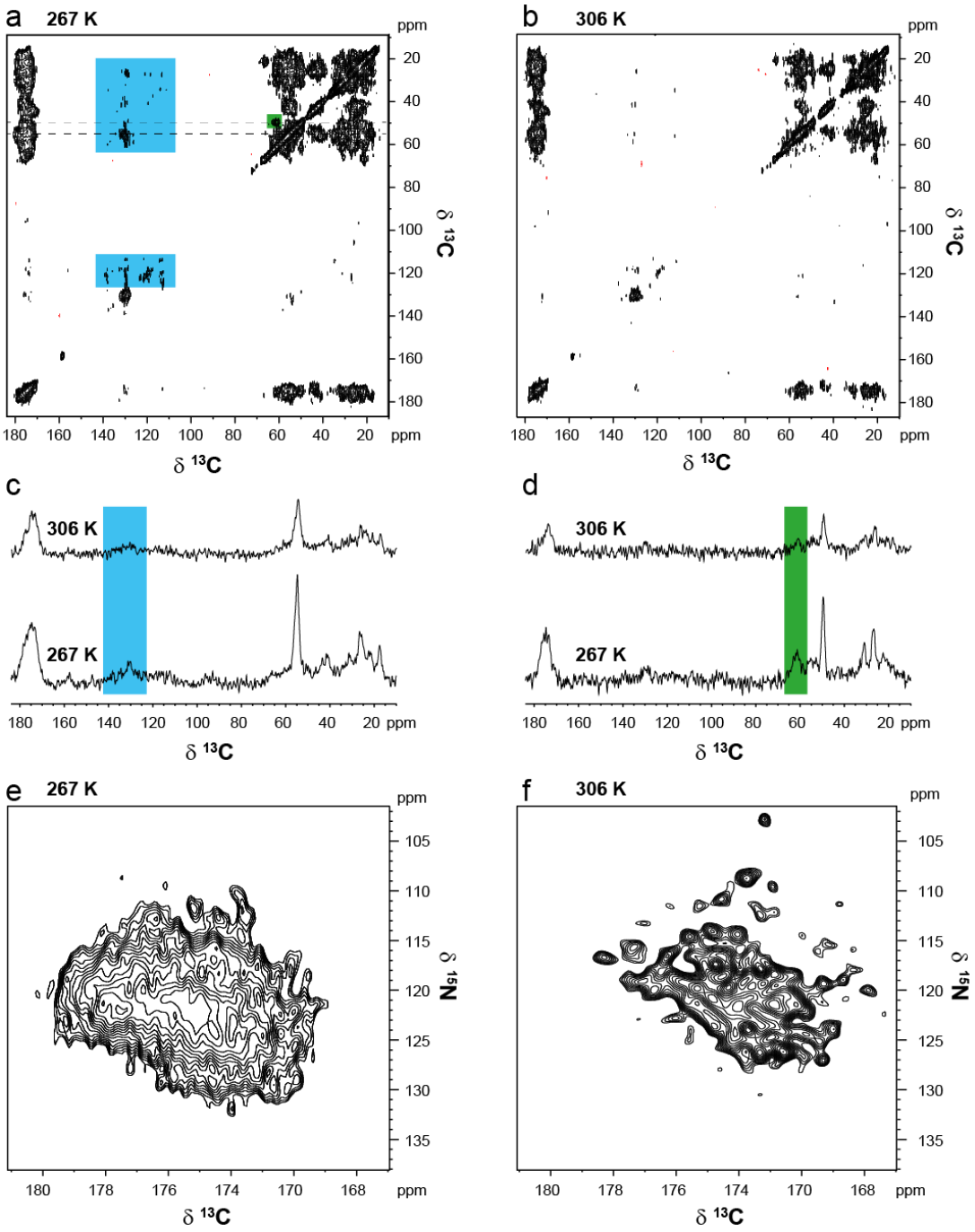

Figure 3: 2D ^{13}C - ^{13}C DARR spectra recorded at 10 kHz MAS with 100 ms mixing (a, b) and ^{15}N - ^{13}CO (e, f) of mTSPO at two temperatures (267 and 306 K). Regions with increased polarization transfer at 267 K are highlighted in blue and green on the DARR spectrum. Two rows (c, d) extracted from the DARR spectra at 267 and 306 K illustrate the improved transfer at 267 K. The following experimental parameters were used in the different spectra: 128 transients, 2s repetition delay for the DARR spectra (a, b); 512 transients, 2s repetition delay for the NCO spectra. The following apodisation functions have been used: cosine square function in the indirect dimension and exponential decay corresponding to 20 Hz line broadening factor for DARR and exponential decay corresponding to 20 Hz line broadening factor in both dimensions for the NCO spectra, respectively.

3.2 Assignment attempt of the residue type of apo TSPO

Like in solution NMR, a prerequisite for sequence-specific resonance assignment by solid-state NMR is the recording of multiple intra- and inter-residue connectivities which can be obtained using 2D and 3D correlation spectra. Transmembrane proteins, like TSPO, comprise structural elements like α-helices which lead to little dispersion for the ^{13}C and ^{15}N resonances hence rendering the specific chemical shift assignment challenging. The task is even more laborious for samples with structural heterogeneity which impairs high resolution.

With ^{15}N CPMAS signal optimized at low temperature for the recording of 2D NCA and NCO spectra, we further attempted to acquire 3D spectra. 3D NCOCX experiments have initially been attempted at 306 K without being able to record an exploitable spectrum due to the fast ^{15}N decay in the nitrogen dimension. A NCOCX spectrum was recorded at 267 K (see Fig S2 for the NCO plane projection of the 3D NCOCX) but only few cross peaks have been observed in agreement with the 2D NCO spectra that showed reduced transfer from N to CO which further limits the transfer to the 3rd dimension via the DARR transfer element. We also endeavoured another strategy (CXCON and CXCAN) starting on carbons, followed by DARR CC mixing with a final transfer from carbons (CO or CA) next to nitrogen by SPECIFIC CP but this failed.

Owing to all these experimental difficulties which have prevented us to get exploitable 3D ^{15}N - ^{13}C - ^{13}C MAS correlation spectra essential for the sequential attribution, we have attempted another attribution strategy based on the use of DARR [37], DQ - SQ [44,50] and PLUQ (PACSYlite Unified Query) [54] to predict amino-acid type regions (Fig 4). PLUQ and previously published solution NMR assignment of mTSPO/PK11195 in detergent have also been exploited to assign the different regions in the DARR spectra. DARR at various mixing times (10, 50 and 100 ms, see Fig 4a-d) were exploited to identify amino-acid specific signals. The amino acids Asp, Asn, Gln, Lys and Ile (Fig S3) have less than five occurrences in the mTSPO protein including the His-tag. Glu, His, Met Phe, Thr and Tyr have between 5 and 10 occurrences whereas Ala, Arg, Gly, Leu, Pro, Ser, Trp and Val have more than 10 occurrences (Fig S3). Cys is not present in the mTSPO sequence. At 10 ms mixing time, we have expected to observe only cross-peaks from one-bond and two-bond correlations. However, at 267 K sample temperature, DARR spectrum shows cross-peaks coming from polarization transfers up to the Cε for some side chains and aromatic residues, including CZ for Tyr (Fig 4a). As mentioned previously for GB1 [37], fluctuations in peak intensity as a function of side-chain topology are observed notably for Thr Cα - Cβ (Fig 4b) for which the intensity is much weaker than that of other Cα - Cβ cross-peaks region. Val Cα - Cβ (Fig 4b) correlations instead seem to be less affected. The observation of cross-peaks coming from more than two-step dipolar transfers and side-chain dependent peak-intensity variation renders difficult the residue type identification in crowded regions. Good agreement with published chemical shifts in detergent is observed for Ala and Arg resonances (Fig 4b, Fig S4). Most of the observed Ala Cα - Cβ cross-peaks correspond to an α-helix structure. Indeed, if we display the Ala residues on the mTSPO/PK11195 structure (PDB ID 2MGY), except Ala102 located in the loop between TM3 & TM4 and Ala168 in the flexible N-terminus, all other Ala residues are in α-helices (3 in TM1, 2 in TM2, 3 in TM3, 5 in TM4 and 4 in TM5). The overlay of

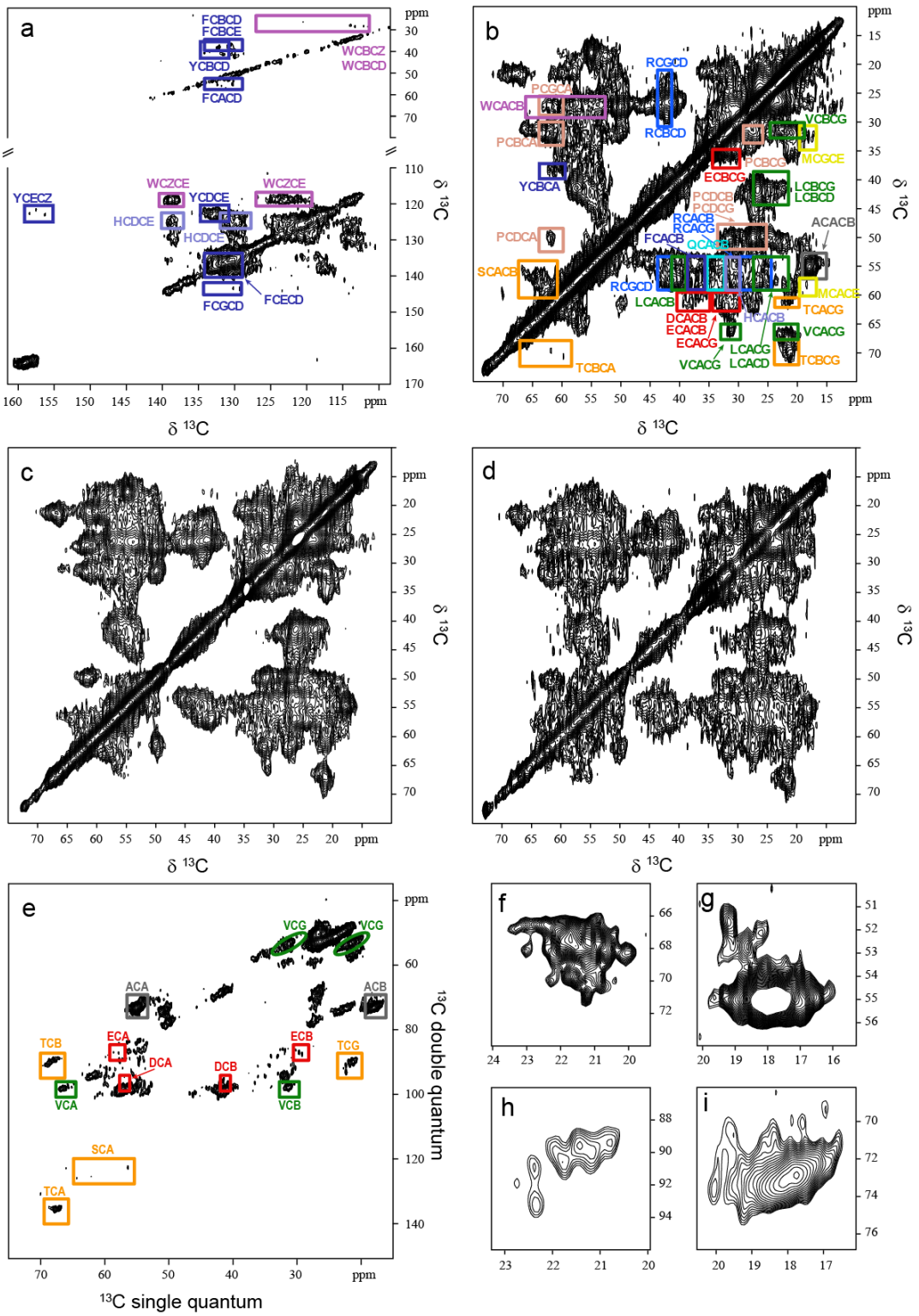

Figure 4: Region assignment of aromatics (a) and aliphatics (b) in a 2D ^{13}C - ^{13}C DARR spectrum at 10 ms mixing. c) Aliphatics region of 2D ^{13}C - ^{13}C DARR spectra at 50 (c) and 100 ms (d) mixing times. e) 2D ^{13}C – ^{13}C DQ – SQ spectrum at 0.48 ms mixing time using the SPC5 block for DQ excitation and reconversion. f-i) Excerpts from 13C – 13C DARR at 10 ms mixing (f, g) and DQ – SQ (h, i) corresponding to TCBCG, VCACG (f), ACACB (g), TCG,CB+CG (h) and ACB,CA+CB. All spectra were recorded at 267 K sample

temperature, 2s repetition time, 256 (DARR 10 ms mixing) or 512 transients (DARR 50 and 100 ms mixing or DQ - SQ) and 10 kHz frequency rate.

the assignment of mTSPO/PK11195 complex in DPC micelles [20] on the spectrum of mTSPO in proteoliposomes shows partial agreements (Fig S4) indicating that the PK11195 ligand considerably influences the structuration of the protein. In addition, it is also expected that the previously published assignment of mTSPO/PK11195 complex cannot be directly transposed to solid-state data owing to differences in environment (detergent micelles for solution NMR versus lipids for ssNMR). However, based on representative strip plots for a series of sequential amino acids of the membrane-embedded mTSPO/DAA1106 complex, Jaipuria et al. [23] showed a correspondence between some resonances of the mTSPO/PK11195 complex in micelles and the mTSPO/DAA1106 system embedded into the membrane. This suggests that ligand binding constraints the mTSPO structure more strongly than lipid environment does.

2D ^{13}C – ^{13}C DQ – SQ spectra are obtained, as the name indicates, by combining a DQ ^{13}C spectrum, generated by the dedicated SPC5 scheme, in the indirect dimension with a SQ ^{13}C spectrum in the direct detection dimension. Fig 4d shows the corresponding spectrum recorded on apo mTSPO in lipids. If the SQ dimension is characterized by coherences evolving at the chemical shift of each individual nucleus, the DQ dimension instead corresponds to coherences that evolve at the sum of the chemical shifts of two ^{13}C nuclei. SPC5 polarization transfer efficiency is not considerably influenced by the chemical shift differences as in DARR but the intensity of the correlations can be affected by molecular dynamics. Double-quantum ^{13}C ssNMR spectroscopy is particularly insightful for probing molecular motion in biomolecules as previously shown on microcrystalline ubiquitin [44]. For uniformly ^{13}C-labelled biomolecules, the polarization transfer in the DQ-recoupling scheme is largely dominated by the strongest (i.e., single-bond) dipolar couplings [64] and can therefore provide information about molecular dynamics. For short mixing times, within 0.25 to 0.5 ms, only cross-peaks arising from one-bond transfers are expected. Indeed, we were not able to identify for mTSPO correlations corresponding to two-bond transfers within the aliphatics and only few two-bond transfers were observed between the carbonyls and the aliphatics. Based on the 2D ^{13}C – ^{13}C SPC5 spectrum (Fig 4d), we were able to identify correlations in the regions (CA, CA+CB) and (CB, CB+CA) for the following residues: Thr (8 cross peaks out of 9 expected), Val (6 out of 12), Ala (11 out of 19), Glu (2 out of 5). Despite the rare occurrence in the mTSPO sequence of Asp (3), Lys (2) and Ile (3) amino acids, they cannot be identified in the SPC5 spectrum. According to liquid NMR assignment (overlay Fig S5) of mTSPO we were able identify V118 CA, CA+CO correlations (Fig S6).

3.3 Conformation heterogeneity and mobility

Conformational heterogeneity and mobility can be probed by DQ ^{13}C ssNMR spectroscopy as shown in Fig 5a on the 2D ^{13}C – ^{13}C DQ-SQ spectra recorded on apo mTSPO in lipids at different mixing times. Indeed, the signal intensity increases with a mixing time from 0.25 (red) to 0.5 ms (blue) and reveals a higher mobility in particular in the CO region. For comparison, the experiment has also been recorded on a sample of GB1 microcrystals (Fig 5b) under the same SPC5 recoupling conditions (i.e., rf irradiation

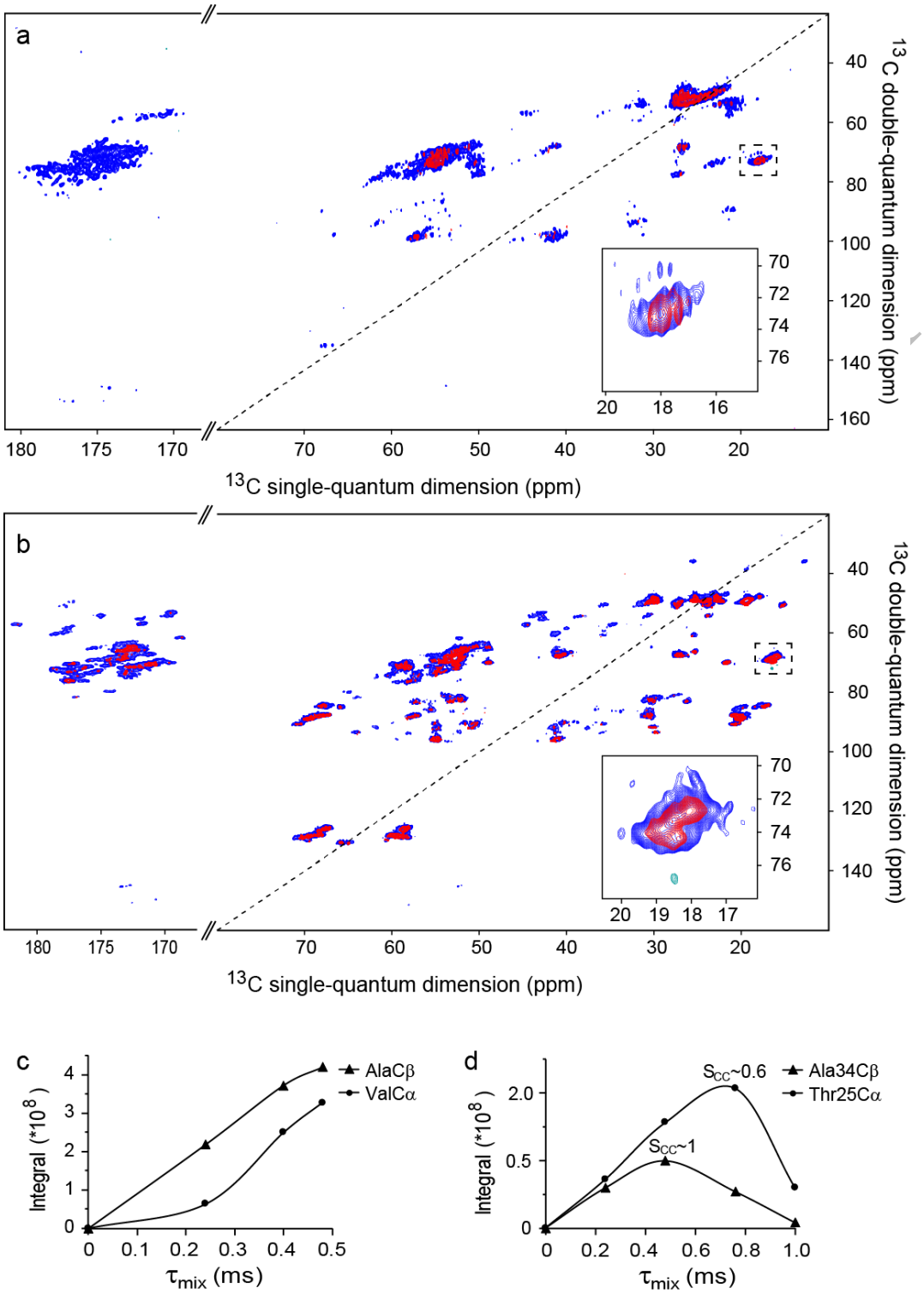

Figure 5: Overlay of 2D ^{13}C - ^{13}C SQ – DQ spectra at 0.25 (red) and 0.5 ms (blue) excitation and reconversion delays of length τ_{mix} each in the SPC5 recoupling scheme for mTSPO reconstituted in liposomes at 267 K (a) and GB1 microcrystals at 280.5 K (b). Excerpts for AlaCB,CA+CB are shown on bottom right-side of each spectrum. Build-up curves for two ^{13}C mTSPO cross-peaks at 267 K (c) and same type ^{13}C GB1 cross-peaks at 295 K (d). The symbols represent the calculated cross-peak volume. All spectra were recorded at 2s repetition time, 512 (mTSPO DQ - SQ) or 128 transients (GB1 DQ – SQ) and 10 kHz frequency rate.

frequency and mixing times) but at a higher temperature. The two spectra of GB1 are very similar, contrary to the mTSPO were only few cross peaks are observed at short mixing time (i.e 0.25 ms) and more correlations become visible by increasing the mixing time (i.e. 0.5ms). The simple evaluation of the intensity of most of the cross peaks show an increase with the mixing time and suggests that these cross-peaks describe mobile residues [44]. Since signals' intensity may be dominated by the CP efficiency or other contributions independent on the DQ excitation scheme, a more accurate analysis relies on the calculation of the cross-peak volumes at each mixing time. Fig 5c and d presents the experimental build up curves for apo mTSPO in lipids and GB1 microcrystals for two amino acid types. The availability of DQ – SQ spectra for mixing times as long as 1 ms for GB1 microcrystals allowed us to model and therefore estimate the order parameters (S_{CC}) using the equation for a three spin system [44,50,64]. The data gained for GB1 allows to identify regions with different mobility like A34 and T25 for example. In the case of mTSPO, we gained qualitative information on the existence of mobility in particular on the backbone since the CO region is particularly affected by the increase of mixing time. However, we were unable to get the Scc of the different region because we lack enough DQ – SQ spectra at mixing time above 0.5 ms under the same experimental conditions in order to accurately model the build-up curves for the double quantum profile.

4. Discussion

While the atomic structure of monomeric mTSPO bound to the high-affinity PK11195 ligand has been determined by solution NMR in DPC detergent micelles [20], ssNMR studies have revealed the dynamic monomer-dimer equilibrium of mTSPO complexed with DAA1106 ligand in DMPC lipids regulated by diamagnetic [23] or paramagnetic [65] cholesterol, another ligand. Rivière et al. [24] studied the influence of 1,2-dinervonoyl-sn-glycero-3-phosphocholine (with an acyl chain monosaturated and longer than DMPC) or a mix of lipids but no resolution improvement of the TSPO/cholesterol ^{13}C – ^{13}C correlation spectra of the was observed for the protein reconstituted in the new membrane mimics. Cholesterol is also a key structural element of mitochondrial membrane and its concentration in the cell membrane varies between 30 and 50 % mole/mole of the entire lipids compounds. In liposomes, cholesterol has been reported to improve their stability and therefore to prevent aggregation. At high cholesterol-TSPO ratio, we may expect that cholesterol molecules will surround mTSPO and therefore displace the equilibrium monomer-dimer. Conversely, we don't know which is the effect of high-affinity cholesterol binding to the CRAC motif at low cholesterol-TSPO ratio with a 1:1 stoichiometry. The dimeric state revealed by Jaipuria et al. [23,65] is in agreement with the different atomic structures gained by crystallography of two bacterial (*Rhodobacter sphaeroides* and *Bacillus cereus*) TSPO in lipid-cubic phase [25,26]. However, apo and holo forms of bacterial TSPO are very similar. This might be linked to the experimental condition since the X-ray data were collected at cryogenic temperatures which are suspected to favour a unique conformation and therefore hide structural ensembles in protein crystals [66].

Temperature is a key parameter to increase ssNMR signal by optimizing the dipolar transfer mechanism. It's worth noting that the regulated temperature is different from the effective sample temperature which increases owing to the heat generated by rotation (Fig

S7). Lower is the chosen temperature, bigger the temperature gradient between the regulated temperature and the real sample temperature. Moreover, there is also a temperature gradient within the rotor that affects the homogeneity within the sample. In ssNMR studies, the slow decrease of sample temperature for systems with structural heterogeneity or disorder leads to the freezing of the whole range of coexisting conformations and therefore favour a considerable broadening of the resonances. However, working at temperatures below lipid phase transition, of DMPC in our case, around 20°C, contributes to the mTSPO signal increase (see Fig 3a, c, d) and therefore to the NMR sensitivity improvement. In addition, the increase of the bound water signal [67] may also contribute to the mTSPO signal enhancement and the efficiency of the polarization transfer and therefore of the cross peaks like clearly visible for the aromatics and the prolines (see Fig 3a). ^{1}H NMR spectra at 313 and 267 K sample temperature (see Fig S8) show that the "free" water is not frozen under the lowest temperature conditions used herein, i.e. -6°C whereas the "bound" water signal broadens. This in agreement with previous studies on microcrystalline samples under very similar rotor size and spinning frequency conditions which show the disappearance of the "free" water signal at -20°C. If the mTSPO in reconstituted lipids has a similar binding cavity filled with water molecules as observed for the *Bc*TSPO crystals [25], this might contribute to the improvement of the polarization transfer under these temperature conditions.

The resolution of the ^{13}C – ^{13}C and ^{15}N – ^{13}C ssNMR spectra (Fig 3 and 4) obtained for apo WT mTSPO in DMPC/DMPE 9/1 w/w liposomes (LPR 1.5 w/w) suggest a conformational-structural heterogeneity. The first term is attributed to a dimer-monomer equilibrium whereas the second describes the double orientation of the protein within the membrane which is characteristic to the reconstitution process, i.e., with almost 50% of the population facing the outside of the liposome and 50% the inside or different percentages depending on the charge of the lipids, pH, etc. In the cell, this could lead to other types of protein-protein interactions as inferred from molecular dynamics [46]. Additionally, it is expected that the protein-protein contacts are favoured and therefore the oligomerization. Nevertheless, the resolution of the obtained ^{13}C – ^{13}C spectra doesn't allow to clearly state if the mTSPO monomer form or dimer form or a monomer-dimer equilibrium is favoured in the absence of the ligand. Instead, the 2D NCO correlation spectra tend to suggest that the peaks appear by pair suggesting at least two conformations, an equilibrium between the monomer and dimer which are expected at the 1.5 w/w LPR used, in agreement with the results previous results by Jaipuria et al. [23]. In the same work, for LPR < 1 w/w, the population of the dimer was estimated at 75% whereas for 1 < LPR < 3 the monomer and dimer forms are in equilibrium with the monomer slightly favoured (dimer ~45%, monomer 55%). In order to compare our ^{13}C – ^{13}C DARR spectra (100 ms) of apo WT mTSPO at 267 and 306 K with those obtained by Rivière et al. [24] (Fig 2 and 3 in their work) under similar temperature conditions, we present in Fig 6 the aliphatic regions of the spectra in Fig 3a and b processed with the same apodisation function in both direct and indirect dimension. Spectra on the right-side of Fig 6 show excerpts corresponding to the Val(CB, CG1/CG2) region and illustrate significantly more correlations at 267 K: if we consider only the Val(CB, CG1), 12 cross-correlation would have expected. Even at an LPR of 1.5 w/w, the lipid chain 4-11 signal with strong wiggles (~ 32 ppm) is observed with 20 Hz line broadening apodisation.

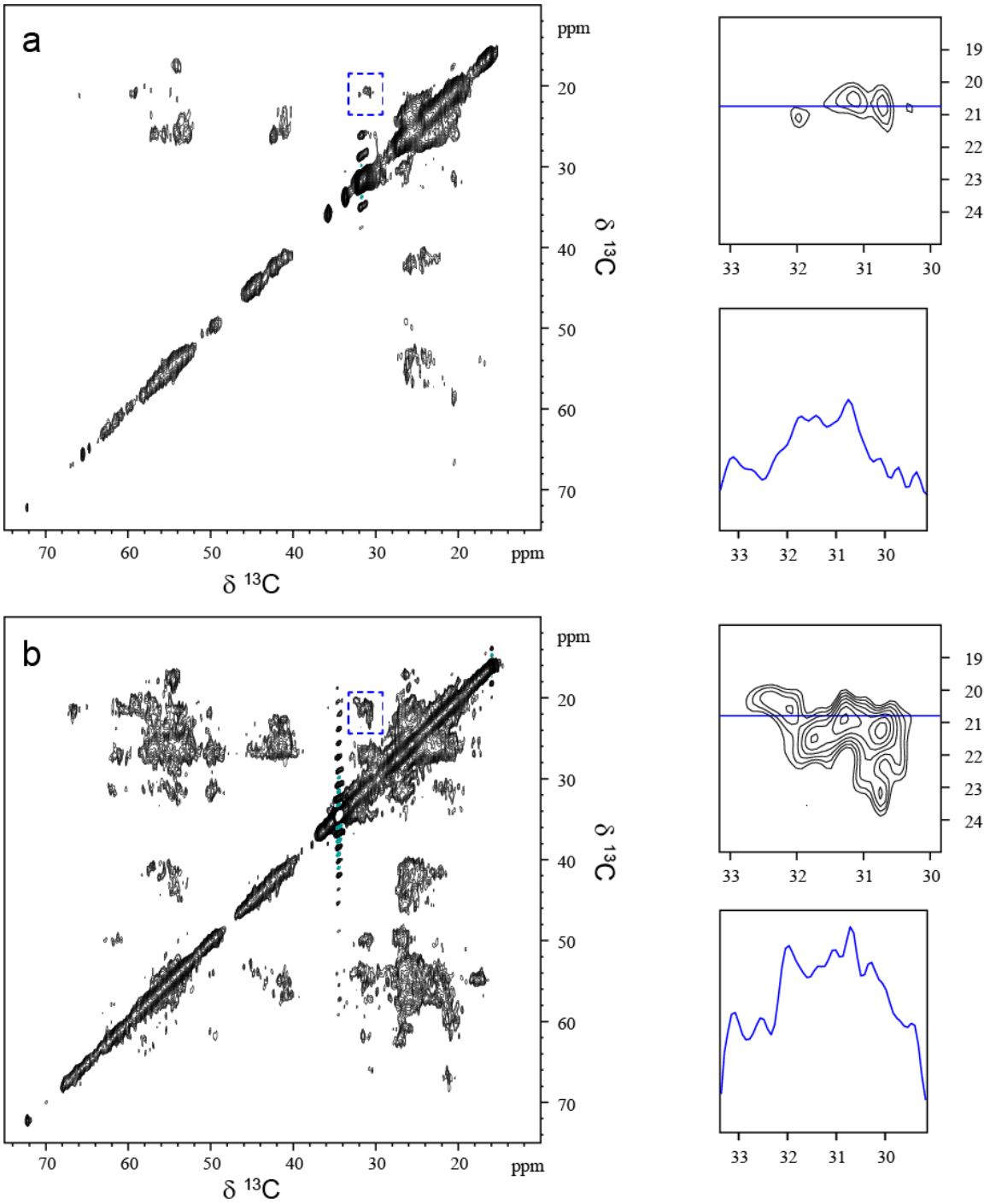

Figure 6: Apo mTSPO 2D ^{13}C - ^{13}C DARR spectra (100 ms) recorded at 10 kHz MAS and 306 (a) and 267 K (b). Val(CB,CG1,CG2) regions in each spectrum are shown on right side for each corresponding temperature together with a row at ~ 21 ppm. The following experimental parameters were used in the different spectra: 128 transients, 2s repetition delay for the DARR spectra, 20 Hz line broadening in both dimensions. The contour level parameters were: ± 65000 lowest intensity, 1.1 increment, 40 contour levels.

Compared to the detergent environment, our results suggest that the lipids environment induces a stabilization of the apo mTSPO protein but the lipids, by themselves, are not enough to determine the protein structure in the absence of the ligand. These results are in agreement with 2D ^{13}C – ^{13}C PDSD spectra at 5°C of mTSPO in DMPC at higher

LPR (50:1, 20:1 molar ratio) in the absence of ligand [23]. It's worth noting that less than 50% of the backbone $^{1}H - ^{15}N$ signals of the mTSPO are broad beyond detection without lipids and in the absence of the ligand independently of the detergent used [21]. Comparison of various detergent environment has shown an important effect upon mTSPO $^{1}H - ^{15}N$ signals dispersion and intensities (Jaremko et al 2015). Thus, further screening of membrane composition or mimics is definitely required to see if a suitable lipid composition capable to stabilize a unique conformation can be identified. Lipids with different lengths and saturation levels have revealed the conformational plasticity of another membrane protein [36]. More generally, membrane mimetics have been shown to be useful to improve ssNMR spectral resolution. Comparison of membrane protein reconstituted either in synthetic lipids or in bacterial cellular envelopes shows a decrease of resolution for the latter, which can be due to the presence of partners that very likely stabilizes different coexisting conformations important for the biological function [68]. TSPO functional state has been described to be linked to interaction with different partners [69]. Thus, the optimization of protein-lipids interactions and/or the presence of functional partner(s) might help in finding stabilizing conditions for mTSPO and in solving the structural heterogeneity.

Residue-specific ssNMR chemical assignments are required to characterize at atomic level the apo mTSPO reconstituted lipid liposomes. Further work exploiting advanced selective isotope labelling possibly combined with a rational optimization of the reconstitution protocol at slightly higher LPR may reduce the spectral crowding and therefore give access to high-resolution 2D and 3D ssNMR spectra. Then, conformational mobility would be better analysed knowing the assignment, in particular for sequential amino acids.

5. Conclusion and perspectives

We have presented herein the optimization of experimental conditions leading to the best currently achievable resolution of MAS ssNMR $^{13}C - ^{13}C$ and $^{15}N - ^{13}C$ spectra of the ligand-free WT mTSPO in DMPC/DMPE 9/1 w/w at a LPR of 1.5. Various ssNMR techniques have been tested and compared to probe the rigid and mobile regions of the lipids or of the protein reconstituted in lipids. Partial assignment of residue types indicates some agreements with the published solution NMR assignment of the PK11195-bound mTSPO in DPC detergent. Overall, the different 2D and 3D experiments recorded for the protein assignment clearly indicate that the apo mTSPO exhibits a high flexibility in a lipid environment. ^{13}C double-quantum NMR spectroscopy further confirmed this remarkable conformational flexibility, which may have significant implications on the recognition of the ligand and/or other protein partners. It has to be mentioned that solution NMR assignment of mTSPO amino acids directly involved in the PK11195 binding reveals the implication of over more than ten residues from the five transmembrane helices [20]. This could explain the gain of stability induced by the binding of the ligand. Moreover, the binding site of bacterial TSPO is also able to bind a very different ligand like porphyrin [26]. This raises the question of the biological significance of such constraints for PK111195 binding site: does the apo form of the mTSPO need a large flexibility to bind so different ligands, such as isoquinoline and porphyrin?

Among the biomolecules of medical interest, membrane proteins such as GPCR suffer from spectral crowding induced by conformational plasticity [70] that, for most of them, limits their access for NMR investigation. High-magnetic field and MAS spinning above 60 kHz rotation frequency demonstrated that sensitivity and ^{1}H resolution can be significantly improved, notably for microcrystalline proteins available in small amounts [71] but also for membrane proteins [41]. Selective ^{13}C-isotope labelling schemes should alleviate the spectral crowding induced by the high percentage of hydrophobic amino acids present in α-helical membrane proteins and therefore, they could help the detection of conformational plasticity of biologically systems by solid-state NMR. Cell-free expression systems are also suited for the study of hydrophobic systems since they enable an amino acid specific labelling slightly more accessible than the use of auxotroph bacterial strains, and partial amino acid labelling like ^{13}C-methyl [72,73]. In addition, the introduction of ^{13}C DQ dimension in 3D proton-detected ssNMR experiments [45] above 60 kHz could facilitate the assignment of these challenging biological systems. Therefore, the combination of all these strategies with multidimensional correlation experiments at high magnetic field, should render accessible the study of even more membrane proteins.

Conflict of interest

The authors declare no conflict of interests.

Author contributions

L.D., L.S., B.P., V.P. and J.-J.L. designed research; L.D., L.S., B.P. and J.-J.L. performed experiments and analysed data; L.D., V.P. and J.-J.L. wrote the paper.

Acknowledgements

This work was financially supported by the CNRS to L.D., B.R. and J.-J.L., Sorbonne-University to B.R. and J.-J.L., and by the Canadian Institutes of Health Research (grant number PJT148659) and the John Stauffer Dean's Chair in Pharmaceutical Sciences (University of Southern California) to V.P.; L.S. was the recipient of a fellowship from the Ministère de la Recherche Française. L.D. acknowledges financial support from the Hauts-de-France Region, the European Regional Development Fund (ERDF) 2014/2020 and Idex Sorbonne Université Investissements d'Avenir (2019/2020 EMERGENCE program).

Appendix. Supplementary data

Supplementary data associated with this article can be found in the online version: 1D ^{13}C INEPT and CPMAS spectra of lipid vesicles and mTSPO in lipids over a range of temperatures; 3D NCOCX; 2D DARR with the solution NMR assignment overlaid; 2D SPC5 with the solution NMR assignment overlaid; Sample temperature versus sensor temperature for the triple 4 mm probe head used in this study.

References

[1] B.C. Choy, R.J. Cater, F. Mancia, E.E. Pryor, A 10-year meta-analysis of membrane protein structural biology: Detergents, membrane mimetics, and structure determination techniques, Biochim. Biophys. Acta - Biomembr. 1863 (2021) 183533. https://doi.org/10.1016/j.bbamem.2020.183533.

[2] A.A. Kermani, A guide to membrane protein X-ray crystallography, FEBS J. (2020) 1–17. https://doi.org/10.1111/febs.15676.

[3] N. Thonghin, V. Kargas, J. Clews, R.C. Ford, Cryo-electron microscopy of membrane proteins, Methods. 147 (2018) 176–186. https://doi.org/10.1016/j.ymeth.2018.04.018.

[4] G.I. Danmaliki, P.M. Hwang, Solution NMR spectroscopy of membrane proteins, Biochim. Biophys. Acta - Biomembr. 1862 (2020) 183356. https://doi.org/10.1016/j.bbamem.2020.183356.

[5] D. Lacabanne, C. Orelle, L. Lecoq, B. Kunert, C. Chuilon, T. Wiegand, S. Ravaud, J.M. Jault, B.H. Meier, A. Böckmann, Flexible-to-rigid transition is central for substrate transport in the ABC transporter BmrA from Bacillus subtilis, Commun. Biol. 2 (2019) 1–9. https://doi.org/10.1038/s42003-019-0390-x.

[6] D. Lacabanne, T. Wiegand, M. Di Cesare, C. Orelle, M. Ernst, J.-M. Jault, B.H. Meier, A. Böckmann, Solid-state NMR Reveals Asymmetric ATP hydrolysis in the Multidrug ABC Transporter BmrA, J. Am. Chem. Soc. 144 (2022) 12431–12442. https://doi.org/10.1021/jacs.2c04287.

[7] E.E. Najbauer, K.T. Movellan, T. Schubeis, T. Schwarzer, K. Castiglione, K. Giller, G. Pintacuda, S. Becker, L.B. Andreas, Probing membrane protein insertion into lipid bilayers by solid-state NMR, ChemPhysChem. 20 (2019) 302–310. https://doi.org/10.1002/cphc.201800793.

[8] S. Xiang, C. Pinto, M. Baldus, Divide and Conquer: A Tailored Solid-state NMR Approach to Study Large Membrane Protein Complexes, Angew. Chem. Int. Ed. 202203319 (2022). https://doi.org/10.1002/anie.202203319.

[9] V.S. Mandala, M.J. McKay, A.A. Shcherbakov, A.J. Dregni, A. Kolocouris, M. Hong, Structure and drug binding of the SARS-CoV-2 envelope protein transmembrane domain in lipid bilayers, Nat. Struct. Mol. Biol. 27 (2020) 1202–1208. https://doi.org/10.1038/s41594-020-00536-8.

[10] E.E. Najbauer, S. Becker, K. Giller, M. Zweckstetter, A. Lange, C. Steinem, B.L. de Groot, C. Griesinger, L.B. Andreas, Structure, gating and interactions of the voltage-dependent anion channel, Eur. Biophys. J. 50 (2021) 159–172. https://doi.org/10.1007/s00249-021-01515-7.

[11] M. Callon, A.A. Malär, S. Pfister, V. Římal, M.E. Weber, T. Wiegand, J. Zehnder, M. Chávez, R. Cadalbert, R. Deb, A. Däpp, M.L. Fogeron, A. Hunkeler, L. Lecoq, A. Torosyan, D. Zyla, R. Glockshuber, S. Jonas, M. Nassal, M. Ernst, A. Böckmann, B.H. Meier, Biomolecular solid-state NMR spectroscopy at 1200 MHz: the gain in resolution, J. Biomol. NMR. 75 (2021) 255–272. https://doi.org/10.1007/s10858-021-00373-x.

[12] E. Nimerovsky, K.T. Movellan, X.C. Zhang, M.C. Forster, E. Najbauer, K. Xue, R. Dervişoğlu, K. Giller, C. Griesinger, S. Becker, L.B. Andreas, Proton detected solid-state nmr of membrane proteins at 28 tesla (1.2 ghz) and 100 khz magic-

angle spinning, Biomolecules. 11 (2021). https://doi.org/10.3390/biom11050752.
[13] D.E. Warschawski, Membrane protein structures determined by NMR, (n.d.). https://www.drorlist.com/nmr/MPNMR.html (accessed March 29, 2022).
[14] A. Loquet, B. Habenstein, Database of membrane protein structures determined by NMR, (n.d.). http://www.loquetlab.org/nmr_mpstruc/ (accessed March 29, 2022).
[15] D.E. Warschawski, M. Traikia, P.F. Devaux, G. Bodenhausen, Solid-state NMR for the study of membrane systems: The use of anisotropic interactions, Biochimie. 80 (1998) 437–450. https://doi.org/10.1016/S0300-9084(00)80011-5.
[16] B. Habenstein, A. Loquet, Solid-state NMR: An emerging technique in structural biology of self-assemblies, Biophys. Chem. 210 (2016) 14–26. https://doi.org/10.1016/j.bpc.2015.07.003.
[17] S.H. White, Membrane proteins of known 3D structure, (n.d.). https://blanco.biomol.uci.edu/mpstruc (accessed March 29, 2022).
[18] N.T. Johansen, M. Bonaccorsi, T. Bengtsen, A.H. Larsen, F.G. Tidemand, M.C. Pedersen, P. Huda, J. Berndtsson, T. Darwish, N.R. Yepuri, A. Martel, T.G. Pomorski, A. Bertarello, M. Sansom, M. Rapp, R. Crehuet, T. Schubeis, K. Lindorff-Larsen, G. Pintacuda, L. Arleth, Mg2+-dependent conformational equilibria in CorA and an integrated view on transport regulation, Elife. 11 (2022). https://doi.org/10.7554/elife.71887.
[19] V. Papadopoulos, M. Baraldi, T.R. Guilarte, T.B. Knudsen, J.J. Lacapère, P. Lindemann, M.D. Norenberg, D. Nutt, A. Weizman, M.R. Zhang, M. Gavish, Translocator protein (18 kDa): new nomenclature for the peripheral-type benzodiazepine receptor based on its structure and molecular function, Trends Pharmacol. Sci. 27 (2006) 402–409. https://doi.org/10.1016/j.tips.2006.06.005.
[20] L. Jaremko, M. Jaremko, K. Giller, S. Becker, M. Zweckstetter, Structure of the mitochondrial translocator protein in complex with a diagnostic ligand, Science. 343 (2014) 1363–1367. https://doi.org/10.1126/science.1248725.
[21] Ł. Jaremko, M. Jaremko, K. Giller, S. Becker, M. Zweckstetter, Conformational Flexibility in the Transmembrane Protein TSPO, Chem. - A Eur. J. 21 (2015) 16555–16563. https://doi.org/10.1002/chem.201502314.
[22] J.J. Lacapère, F. Delavoie, H. Li, G. Péranzi, J. Maccario, V. Papadopoulos, B. Vidic, Structural and functional study of reconstituted peripheral benzodiazepine receptor, Biochem. Biophys. Res. Commun. 284 (2001) 536–541. https://doi.org/10.1006/bbrc.2001.4975.
[23] G. Jaipuria, A. Leonov, K. Giller, S.K. Vasa, Á. Jaremko, M. Jaremko, R. Linser, S. Becker, M. Zweckstetter, Cholesterol-mediated allosteric regulation of the mitochondrial translocator protein structure, Nat. Commun. 8 (2017) 1–8. https://doi.org/10.1038/ncomms14893.
[24] G. Rivière, G. Jaipuria, L.B. Andreas, A. Leonov, K. Giller, S. Becker, M. Zweckstetter, Membrane-embedded TSPO: an NMR view, Eur. Biophys. J. (2020). https://doi.org/10.1007/s00249-020-01487-0.
[25] Y. Guo, R.C. Kalathur, Q. Liu, B. Kloss, R. Bruni, C. Ginter, E. Kloppmann, B. Rost, W.A. Hendrickson, Structure and activity of tryptophan-rich TSPO proteins, Science. 347 (2015) 551–5. https://doi.org/10.1126/science.aaa1534.
[26] F. Li, J. Liu, Y. Zheng, R.M. Garavito, S. Ferguson-Miller, Crystal structures of translocator protein (TSPO) and mutant mimic of a human polymorphism,

Science. 347 (2015) 555–558. https://doi.org/10.1126/science.1260590.
[27] J.J. Lacapere, L. Duma, S. Finet, M. Kassiou, V. Papadopoulos, Insight into the structural features of TSPO: Implications for drug development, Trends Pharmacol. Sci. 41 (2020) 110–122. https://doi.org/10.1016/j.tips.2019.11.005.
[28] C. Toyoshima, M. Nakasako, H. Nomura, H. Ogawa, Structure determination of the calcium pump of sarcoplasmic reticulum at 2.6 A resolution, Nature. 46 (2001) 1374–80. http://www.ncbi.nlm.nih.gov/pubmed/11519177.
[29] D. Teboul, S. Beaufils, J.C. Taveau, S. Iatmanen-Harbi, A. Renault, C. Venien-Bryan, V. Vie, J.J. Lacapere, Mouse TSPO in a lipid environment interacting with a functionalized monolayer, Biochim. Biophys. Acta - Biomembr. 1818 (2012) 2791–2800. https://doi.org/10.1016/j.bbamem.2012.06.020.
[30] L. Senicourt, L. Duma, V. Papadopoulos, J.J. Lacapere, Solid-state NMR of membrane protein reconstituted in proteoliposomes: the case of TSPO, in: J.J. Lacapère (Ed.), Membr. Protein Struct. Funct. Charact., Springer Protocols, Humana Press, 2017: pp. 328–344.
[31] M.A. Ostuni, L. Issop, G. Péranzi, F. Walker, M. Fasseu, C. Elbim, V. Papadopoulos, J.J. Lacapere, Overexpression of translocator protein in inflammatory bowel disease: Potential diagnostic and treatment value, Inflamm. Bowel Dis. 16 (2010) 1476–1487. https://doi.org/10.1002/ibd.21250.
[32] J.J. Lacapere, S. Iatmanen-Harbi, L. Senicourt, O. Lequin, P. Tekely, R.N. Purusottam, P. Hellwig, S. Kriegel, S. Ravaud, C. Juillan-Binard, E.P. Peyroula, V. Papadopoulos, Structural studies of TSPO, a mitochondiral membrane protein, in: I. Mus-Veteau (Ed.), Membr. Proteins Prod. Struct. Anal., Springer, 2014: pp. 393–421.
[33] K. Takegoshi, S. Nakamura, T. Terao, 13C-1H dipolar-assisted rotational resonance in magic-angle spinning NMR, Chem. Phys. Lett. 344 (2001) 631–637. https://doi.org/10.1016/S0009-2614(01)00791-6.
[34] M. Baldus, A.T. Petkova, J. Herzfeld, R.G. Griffin, Cross polarization in the tilted frame: Assignment and spectral simplification in heteronuclear spin systems, Mol. Phys. 95 (1998) 1197–1207. https://doi.org/10.1080/00268979809483251.
[35] T. Gopinath, G. Veglia, Proton-detected polarization optimized experiments (POE) using ultrafast magic angle spinning solid-state NMR: Multi-acquisition of membrane protein spectra, J. Magn. Reson. 310 (2020) 106664. https://doi.org/10.1016/j.jmr.2019.106664.
[36] T. Sinnige, M. Weingarth, M. Renault, L. Baker, J. Tommassen, M. Baldus, Solid-State NMR studies of full-length BamA in lipid bilayers suggest limited overall POTRA mobility, J. Mol. Biol. 426 (2014) 2009–2021. https://doi.org/10.1016/j.jmb.2014.02.007.
[37] W.T. Franks, D.H. Zhou, B.J. Wylie, B.G. Money, D.T. Graesser, H.L. Frericks, G. Sahota, C.M. Rienstra, Magic-angle spinning solid-state NMR spectroscopy of the β1 immunoglobulin binding domain of protein G (GB1): 15N and 13C chemical shift assignments and conformational analysis, J. Am. Chem. Soc. 127 (2005) 12291–12305. https://doi.org/10.1021/ja044497e.
[38] B.B. Das, H. Zhang, S.J. Opella, Dipolar Assisted Assignment Protocol (DAAP) for MAS solid-state NMR of rotationally aligned membrane proteins in phospholipid bilayers, J. Magn. Reson. 242 (2014) 224–232.

https://doi.org/10.1016/j.jmr.2014.02.018.
[39] S.H. Park, B.B. Das, F. Casagrande, Y. Tian, H.J. Nothnagel, M. Chu, H. Kiefer, K. Maier, A.A. De Angelis, F.M. Marassi, S.J. Opella, Structure of the chemokine receptor CXCR1 in phospholipid bilayers, Nature. 491 (2012) 779–783. https://doi.org/10.1038/nature11580.
[40] V.S. Mandala, J.K. Williams, M. Hong, Structure and dynamics of membrane proteins from solid-state NMR, Annu. Rev. Biophys. 47 (2018) 201–222. https://doi.org/10.1146/annurev-biophys-070816-033712.
[41] T. Gopinath, D. Weber, S. Wang, E. Larsen, G. Veglia, Solid-state NMR of membrane Proteins in lipid bilayers: to spin or not to spin?, Acc. Chem. Res. (2021). https://doi.org/10.1021/acs.accounts.0c00670.
[42] A.L. Webber, A.J. Pell, E. Barbet-Massin, M.J. Knight, I. Bertini, I.C. Felli, R. Pierattelli, L. Emsley, A. Lesage, G. Pintacuda, Combination of DQ and ZQ coherences for sensitive through-bond NMR correlation experiments in biosolids under ultra-fast MAS, ChemPhysChem. 13 (2012) 2405–2411. https://doi.org/10.1002/cphc.201200099.
[43] L.J. Sperling, D.A. Berthold, T.L. Sasser, V. Jeisy-Scott, C.M. Rienstra, Assignment strategies for large proteins by magic-angle spinning NMR: The 21-kDa disulfide-bond-forming enzyme DsbA, J. Mol. Biol. 399 (2010) 268–282. https://doi.org/10.1016/j.jmb.2010.04.012.
[44] R. Schneider, K. Seidel, M. Etzkorn, A. Lange, S. Becker, M. Baldus, Probing molecular motion by double-quantum (13C,13C) solid-state NMR spectroscopy: Application to ubiquitin, J. Am. Chem. Soc. 132 (2010) 223–233. https://doi.org/10.1021/ja906283h.
[45] A. Lends, M. Berbon, B. Habenstein, Y. Nishiyama, A. Loquet, Protein resonance assignment by solid-state NMR based on 1H-detected 13C double-quantum spectroscopy at fast MAS, J. Biomol. NMR. 75 (2021) 417–427. https://doi.org/10.1007/s10858-021-00386-6.
[46] R. Rao, J. Diharce, B. Dugué, M.A. Ostuni, F. Cadet, C. Etchebest, Versatile dimerisation process of translocator protein (TSPO) revealed by an extensive sampling based on a coarse-grained dynamics study, J. Chem. Inf. Model. 60 (2020) 3944–3957. https://doi.org/10.1021/acs.jcim.0c00246.
[47] M.A. Ostuni, S. Iatmanen, D. Teboul, J.-C. Robert, J.-J. Lacapère, Characterization of membrane protein preparations: Measurement of detergent content and ligand binding after proteoliposomes reconstitution, in: J.-J. Lacapère (Ed.), Membr. Protein Struct. Determ. Methods Protoc., Humana Press, Totowa, NJ, 2010: pp. 3–18. https://doi.org/10.1007/978-1-60761-762-4_1.
[48] M. Günther, W. Xiaoling, S.O. Smith, Ramped-amplitude cross polarization in magic-angle-spinning NMR, J. Magn. Reson. Ser. A. 110 (1994) 219–227.
[49] B.M. Fung, A.K. Khitrin, K. Ermolaev, An improved broadband decoupling sequence for liquid crystals and solids, J. Magn. Reson. 142 (2000) 97–101. https://doi.org/10.1006/jmre.1999.1896.
[50] M. Hohwy, C.M. Rienstra, C.P. Jaroniec, R.G. Griffin, Fivefold symmetric homonuclear dipolar recoupling in rotating solids: Application to double quantum spectroscopy, J. Chem. Phys. 110 (1999) 7983–7992. https://doi.org/10.1063/1.478702.

[51] F. Delaglio, S. Grzesiek, G.W. Vuister, G. Zhu, J. Pfeifer, A. Bax, NMRPipe: A multidimensional spectral processing system based on UNIX pipes, J. Biomol. NMR. 6 (1995) 277–293. https://doi.org/10.1007/BF00197809.
[52] W. Lee, M. Tonelli, J.L. Markley, NMRFAM-SPARKY: Enhanced software for biomolecular NMR spectroscopy, Bioinformatics. 31 (2015) 1325–1327. https://doi.org/10.1093/bioinformatics/btu830.
[53] S. Gradmann, C. Ader, I. Heinrich, D. Nand, M. Dittmann, A. Cukkemane, M. Van Dijk, A.M.J.J. Bonvin, M. Engelhard, M. Baldus, Rapid prediction of multi-dimensional NMR data sets, J. Biomol. NMR. 54 (2012) 377–387. https://doi.org/10.1007/s10858-012-9681-y.
[54] K.J. Fritzsching, Y. Yang, K. Schmidt-Rohr, M. Hong, Practical use of chemical shift databases for protein solid-state NMR: 2D chemical shift maps and amino-acid assignment with secondary-structure information, J. Biomol. NMR. 56 (2013) 155–167. https://doi.org/10.1007/s10858-013-9732-z.
[55] M.W. Maciejewski, A.D. Schuyler, M.R. Gryk, I.I. Moraru, P.R. Romero, E.L. Ulrich, H.R. Eghbalnia, M. Livny, F. Delaglio, J.C. Hoch, NMRbox: A Resource for biomolecular NMR computation, Biophys. J. 112 (2017) 1529–1534. https://doi.org/10.1016/j.bpj.2017.03.011.
[56] A. Bielecki, D.P. Burum, Temperature dependence of 207Pb MAS spectra of solid lead nitrate. An accurate, sensitive thermometer for variable-temperature MAS, J. Magn. Reson. Ser. A. 116 (1995) 215–220. https://doi.org/10.1006/jmra.1995.0010.
[57] S. V. Dvinskikh, K. Yamamoto, U.H.N. Dürr, A. Ramamoorthy, Sensitivity and resolution enhancement in solid-state NMR spectroscopy of bicelles, J. Magn. Reson. 184 (2007) 228–235. https://doi.org/10.1016/j.jmr.2006.10.004.
[58] R.N. Purusottam, L. Sénicourt, J.J. Lacapère, P. Tekely, Probing the gel to liquid-crystalline phase transition and relevant conformation changes in liposomes by13C magic-angle spinning NMR spectroscopy, Biochim. Biophys. Acta - Biomembr. 1848 (2015) 3134–3139. https://doi.org/10.1016/j.bbamem.2015.09.011.
[59] B.A. Lewis, G.S. Harbison, J. Herzfeld, R.G. Griffin, NMR structural analysis of a membrane protein: Bacteriorhodopsin peptide backbone orientation and motion, Biochemistry. 24 (1985) 4671–4679. https://doi.org/10.1021/bi00338a029.
[60] S.H. Park, B.B. Das, A.A. De Angelis, M. Scrima, S.J. Opella, Mechanically, magnetically, and "rotationally aligned" membrane proteins in phospholipid bilayers give equivalent angular constraints for NMR structure determination, J. Phys. Chem. B. 114 (2010) 13995–14003. https://doi.org/10.1021/jp106043w.
[61] K. Ohgo, W.P. Niemczura, B.C. Seacat, S.G. Wise, A.S. Weiss, K.K. Kumashiro, Resolving nitrogen-15 and proton chemical shifts for mobile segments of elastin with two-dimensional NMR spectroscopy, J. Biol. Chem. 287 (2012) 18201–18209. https://doi.org/10.1074/jbc.M111.285163.
[62] K. Takegoshi, S. Nakamura, T. Terao, 13C-1H dipolar-driven 13C-13C recoupling without 13C rf irradiation in nuclear magnetic resonance of rotating solids, J. Chem. Phys. 118 (2003) 2325–2341. https://doi.org/10.1063/1.1534105.
[63] T. Bauer, C. Dotta, L. Balacescu, J. Gath, A. Hunkeler, A. Böckmann, B.H. Meier, Line-broadening in low-temperature solid-state NMR spectra of fibrils, J. Biomol. NMR. 67 (2017) 51–61. https://doi.org/10.1007/s10858-016-0083-4.

[64] M. Baldus, Correlation experiments for assignment and structure elucidation of immobilized polypeptides under magic angle spinning, Prog. Nucl. Magn. Reson. Spectrosc. 41 (2002) 1–47. https://doi.org/10.1016/S0079-6565(02)00007-9.
[65] G. Jaipuria, K. Giller, A. Leonov, S. Becker, M. Zweckstetter, Insights into cholesterol/membrane protein interactions using paramagnetic solid-state NMR, Chem. - A Eur. J. (2018) 17606–17611. https://doi.org/10.1002/chem.201804550.
[66] J.S. Fraser, H. Van Den Bedem, A.J. Samelson, P.T. Lang, J.M. Holton, N. Echols, T. Alber, Accessing protein conformational ensembles using room-temperature X-ray crystallography, Proc. Natl. Acad. Sci. U. S. A. 108 (2011) 16247–16252. https://doi.org/10.1073/pnas.1111325108.
[67] A. Böckmann, C. Gardiennet, R. Verel, A. Hunkeler, A. Loquet, G. Pintacuda, L. Emsley, B.H. Meier, A. Lesage, Characterization of different water pools in solid-state NMR protein samples, J. Biomol. NMR. 45 (2009) 319–327. https://doi.org/10.1007/s10858-009-9374-3.
[68] L.A. Baker, M. Baldus, Characterization of membrane protein function by solid-state NMR spectroscopy, Curr. Opin. Struct. Biol. 27 (2014) 48–55. https://doi.org/10.1016/j.sbi.2014.03.009.
[69] C. Hiser, B.L. Montgomery, S.F. Miller, TSPO protein binding partners in bacteria, animals, and plants, (2021).
[70] T. Laeremans, Z.A. Sands, P. Claes, A. De Blieck, S. De Cesco, S. Triest, A. Busch, D. Felix, A. Kumar, V.-P. Jaakola, C. Menet, Accelerating GPCR drug discovery with conformation-stabilizing VHHs, Front. Mol. Biosci. 9 (2022) 1–21. https://doi.org/10.3389/fmolb.2022.863099.
[71] A. Böckmann, M. Ernst, B.H. Meier, Spinning proteins, the faster, the better?, J. Magn. Reson. 253 (2015) 71–79. https://doi.org/10.1016/j.jmr.2015.01.012.
[72] F. Bernhard, Y. Tozawa, Cell-free expression-making a mark, Curr. Opin. Struct. Biol. 23 (2013) 374–380. https://doi.org/10.1016/j.sbi.2013.03.012.
[73] M. Lazarova, F. Löhr, R.B. Rues, R. Kleebach, V. Dötsch, F. Bernhard, Precursor-based selective methyl labeling of cell-free synthesized proteins, ACS Chem. Biol. 13 (2018) 2170–2178. https://doi.org/10.1021/acschembio.8b00338.